

## One-neutron pickup into $^{49}\text{Ca}$ : Bound neutron $g_{9/2}$ spectroscopic strength at $N = 29$

A. Gade,<sup>1,2</sup> J. A. Tostevin,<sup>3</sup> V. Bader,<sup>1,2</sup> T. Baugher,<sup>1,2</sup> D. Bazin,<sup>1</sup> J. S. Berryman,<sup>1</sup> B. A. Brown,<sup>1,2</sup> D. J. Hartley,<sup>4</sup> E. Lunderberg,<sup>1,2</sup> F. Recchia,<sup>1</sup> S. R. Stroberg,<sup>1,2</sup> Y. Utsuno,<sup>5,6</sup> D. Weisshaar,<sup>1</sup> and K. Wimmer<sup>1,7,\*</sup>

<sup>1</sup>National Superconducting Cyclotron Laboratory, Michigan State University, East Lansing, Michigan 48824, USA

<sup>2</sup>Department of Physics and Astronomy, Michigan State University, East Lansing, Michigan 48824, USA

<sup>3</sup>Department of Physics, University of Surrey, Guildford, Surrey GU2 7XH, United Kingdom

<sup>4</sup>Department of Physics, U.S. Naval Academy, Annapolis, Maryland 21402, USA

<sup>5</sup>Advanced Science Research Center, Japan Atomic Energy Agency, Tokai, Ibaraki 319-1195, Japan

<sup>6</sup>Center for Nuclear Study, University of Tokyo, Hongo, Bunkyo-ku, Tokyo 113-0033, Japan

<sup>7</sup>Department of Physics, Central Michigan University, Mount Pleasant, Michigan 48859, USA

(Received 24 November 2015; revised manuscript received 18 January 2016; published 14 March 2016)

The highly selective, intermediate-energy heavy-ion-induced neutron-pickup reaction, in combination with  $\gamma$ -ray spectroscopy using the  $\gamma$ -ray energy-tracking in-beam nuclear array (GRETINA), is shown to provide reliable relative spectroscopic strengths for high- $\ell$  orbitals in nuclei more neutron rich than the projectile. The reaction mechanism gives a significant final-state-spin alignment that is validated through  $\gamma$ -ray angular-distribution measurements enabled by the position sensitivity of GRETINA. This is the first time that  $\gamma$ -ray angular distributions could be extracted from a high-luminosity, fast-beam reaction other than inelastic scattering. This holds great promise for the restriction and assignment of  $J^\pi$  quantum numbers in exotic nuclei. We advance this approach to study the crucial  $N = 28$  shell closure and extract the ratio  $g_{9/2} : f_{5/2}$  of bound neutron single-particle strengths in  $^{49}\text{Ca}$ , a benchmark for emerging multi-shell *ab initio* and configuration-interaction theories that are applicable along the Ca isotopic chain.

DOI: [10.1103/PhysRevC.93.031601](https://doi.org/10.1103/PhysRevC.93.031601)

The quest for a predictive model of atomic nuclei fuels nuclear science research programs worldwide. The properties of rare isotopes emerge as crucial ingredients for the development of nuclear models whose validity extends towards the nucleon driplines. Many important aspects of the interactions between the constituent protons and neutrons are amplified in neutron-rich nuclei and can best be isolated and characterized there. Light and medium-mass nuclei far away from stability are produced efficiently by projectile fragmentation. The resulting rare-isotope beams are then available for inverse-kinematics experiments at velocities of several tens of percent of the speed of light. Sensitive new experimental techniques have been developed over the years that combine in-beam  $\gamma$ -ray spectroscopy and thick reaction targets, restoring luminosity to enable experimental studies with low-intensity fast rare-isotope beams [1].

Gamma-ray tagged neutron-adding transfer reactions at high beam velocities have only been explored since 2011 [2]. A key property, which we exploit here, is that the fast neutron-pickup process is poorly matched in either the transferred angular or linear momentum at our beam energies, in the sense used in semiclassical model discussions of transfer reactions between heavy ions [3,4]. This leads to a very high selectivity in terms of the orbital angular momentum  $\ell$  of the final states populated. It also introduces a significant anisotropy in the population of the  $M$  substates of the final state (spin alignment), giving rise to significant  $\gamma$ -ray angular distributions that can be used to restrict or assign  $J^\pi$  values

to states in exotic nuclei. Gamma-ray angular distributions from low-energy reactions performed in normal kinematics have provided a wealth of spectroscopic information on nuclei for more than 60 years. In reactions of high-luminosity fast beams, such capabilities have been demonstrated to date only for inelastic scattering measurements [1,5].

Here we report the results of a  $\gamma$ -tagged, inverse kinematics  $^{12}\text{C}(^{48}\text{Ca}, ^{49}\text{Ca} + \gamma)$  transfer reaction study and deduce the neutron  $g_{9/2} : f_{5/2}$  relative spectroscopic strengths at  $N = 29$  in the much-studied Ca isotopic chain. Because  $^{48}\text{Ca}$  is stable, light-ion-induced neutron-adding transfer reactions have previously been measured. However, as a result of the energy doublet of the  $5/2^-$  (3991 keV) and  $9/2^+$  (4018 keV) bound states, which carry the strongest spectroscopic strength, these strengths are obscured for the traditional particle-tagged ( $d, p$ ) transfer reactions; see, e.g., Ref. [6]. We show that, at our beam energy, the inverse-kinematics reaction on  $^{12}\text{C}$  selectively populates these  $^{49}\text{Ca}$  final states with orbital angular momenta  $\ell = 3$  and  $\ell = 4$ . This final-state selectivity, combined with  $\gamma$ -ray spectroscopy of the strongest  $\gamma$ -ray branch (660 keV) of the key  $^{49}\text{Ca}(9/2^+, 4.018 \text{ MeV})$  state, reduces the uncertainty due to the  $5/2^-$  and  $9/2^+$  energy doublet. Furthermore, we show that this reaction mechanism predicts significant final-state spin alignments that allow the  $\gamma$ -ray angular distributions to be exploited for the confirmation of spin and parity ( $J^\pi$ ) assignments in exotic nuclei. This new determination of the relative  $\nu g_{9/2} : \nu f_{5/2}$  spectroscopic strengths in  $^{49}\text{Ca}$  provides an important benchmark for the many models that now tackle the semimagic Ca isotopic chain.

Excited states in  $^{49}\text{Ca}$  were populated in the  $^{12}\text{C}(^{48}\text{Ca}, ^{49}\text{Ca} + \gamma)X$  neutron-pickup reaction, performed at

\*Present address: Department of Physics, The University of Tokyo, Hongo, Bunkyo-ku, Tokyo 113-0033, Japan.

the Coupled Cyclotron Facility at the National Superconducting Cyclotron Laboratory (NSCL). The 140 MeV/u  $^{48}\text{Ca}$  primary beam was energy degraded in the A1900 fragment separator [7] with a 1363 mg/cm $^2$   $^9\text{Be}$  target and transmitted to the experimental vault with the momentum acceptance  $\Delta p/p$  restricted to 0.25%.

The secondary  $^{12}\text{C}$  reaction target (149.4 mg/cm $^2$  thick vitreous carbon with a density of 1.54 g/cm $^3$ , 98.9% enriched in  $^{12}\text{C}$ ) was located at the target position of the S800 spectrograph [8]. The mid-target energy was 66.7 MeV/u. Reaction products were identified on an event-by-event basis at the instrument's focal plane.

The  $\gamma$ -ray energy-tracking in-beam nuclear array (GRETINA), a segmented high-resolution  $\gamma$ -ray detection system [9], was used to measure the prompt  $\gamma$  rays emitted by the reaction residues. The seven GRETINA modules—with four 36-fold segmented crystals each—were arranged in two rings. Four modules were located at 58° and three at 90° with respect to the beam axis. Online signal decomposition provided  $\gamma$ -ray interaction points for event-by-event Doppler reconstruction of the  $\gamma$  rays emitted in-flight. The information on the momentum vector of the projectile-like residues was incorporated into the Doppler reconstruction (see Fig. 1).

The in-beam  $\gamma$ -ray spectrum displayed in Fig. 1 is exceptionally clean, with four intense peak structures visible on rather little background. The inset shows the spectrum on a logarithmic scale to highlight transitions from weakly populated states. The low density of states populated in  $^{49}\text{Ca}$  is inherent to the selectivity of the reaction mechanism employed, as discussed later. The absence of the often-observed in-beam background is attributed to the two-body nature of the reaction, which leaves bound  $^{11}\text{C}$  in the exit channel without light particles emerging from the target that may interact with surrounding material and causing time-prompt background, as investigated recently for nucleon-knockout reactions [10].

For clean particle identification,  $\gamma$ -ray coincidences were required to eliminate an estimated 10%–15% tail of unreacted  $^{48}\text{Ca}$  contaminating identifications made without coincidences. Due to this small projectile beam contamination,

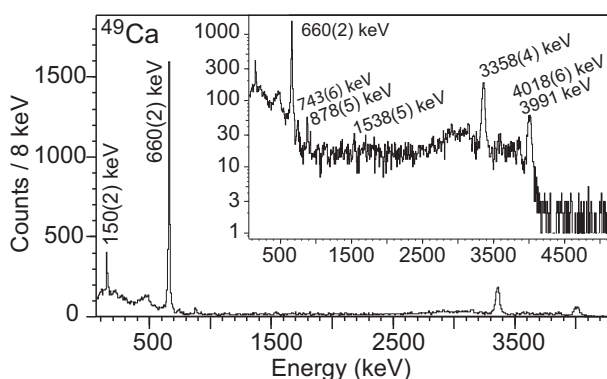


FIG. 1. Doppler-reconstructed  $\gamma$ -ray spectra in coincidence with  $^{49}\text{Ca}$  reaction residues. The inset magnifies the low-statistics transitions from very weakly populated states. The statistics corresponds to about 4.5 hours of data taken at  $3 \times 10^5$   $^{48}\text{Ca}/\text{s}$ .

absolute partial cross sections can be cleanly extracted for the excited states, but only an upper limit can be set for the inclusive and ground-state cross sections ( $\sigma_{\text{inc}} \leq 2.15$  mb). All states and transitions in the observed level scheme have been reported before [11–13]. We point out that the 3358 keV level was reported as  $(9/2^+)$  in the most recent  $(d, p)$  transfer measurement [6], as well as in Ref. [11]. Here, we are able to confirm the  $7/2^-$  assignment recently proposed in Refs. [12,13].

As the high selectivity seen in the measurement and the interpretation of results are closely tied to the reaction mechanism, we first discuss the reaction calculations. At the beam energy of the experiment, the direct neutron-pickup reaction on  $^{12}\text{C}$  is highly angular-momentum mismatched for low- $\ell$  transfers, and the reaction selects transitions with larger orbital angular momenta; see, e.g., Refs. [3,4]. Such selectivity was noted and exploited previously in normal kinematics, carbon-induced nucleon transfer reactions on stable targets at energies of 40–50 MeV/u; see, e.g., Refs. [14,15] and references therein. Here, as there, the neutron transfers are calculated by assuming a single-step mechanism from the ground state of the  $^{12}\text{C}$  target to bound-neutron single-particle states built on the  $^{48}\text{Ca}(\text{g.s.})$  (where “g.s.” means “ground state”). Both the entrance and exit channels are described in terms of bound two-body systems.

We compute the post form of the distorted waves Born approximation (DWBA) transition amplitude using the direct-reactions code FRESKO [16]. Thus, the transfer interaction is that which binds the neutron and  $^{11}\text{C}$  residues, which is treated in finite-range. The reactions are computed as  $^{48}\text{Ca}(^{12}\text{C}, ^{11}\text{C}(I^\pi))^{49}\text{Ca}(J^\pi)$ , populating the  $I^\pi = 3/2_1^-(\text{g.s.})$ ,  $1/2_1^-(2.0 \text{ MeV})$ , and  $3/2_2^-(4.8 \text{ MeV})$  states of  $^{11}\text{C}$ . The measured  $^{49}\text{Ca}(J^\pi)$  cross sections presented here are inclusive with respect to  $^{11}\text{C}(I^\pi)$  final states, so these (incoherent) calculated cross sections to each  $I^\pi$  are summed.

The spectroscopic factors (SFs) for nucleon removal from  $^{12}\text{C}$  are taken from the final-state-exclusive  $(e, e'p)$  proton-knockout analyses, as shown in Table 8 of Ref. [17]. These measured  $3/2_1^-$ ,  $1/2_1^-$ , and  $3/2_2^-$  SFs, of 1.72(11), 0.26(2), and 0.20(2), are used here for neutron removal, given the good  $T = 0$  nature of the  $^{12}\text{C}$  system. Transfer to the  $^{11}\text{C}$  ground state dominates. These empirical SFs essentially agree with those from the shell model [e.g., with the  $p$ - $sd$  Hamiltonian of Warburton and Brown (WBP) [18] of 3.16, 0.58, and 0.19] after scaling the shell-model SF by the measured  $p$ - and  $n$ -removal reduction factors, of 0.53(2) and 0.49(2), deduced from inclusive nucleon removal cross sections from  $^{12}\text{C}$  [19]. In combination with the WBP shell-model SF, this reduction yields a total proton removal strength from  $^{12}\text{C}$  of 2.08(8), compared with the value 2.18(15) of the  $(e, e'p)$  SF of Ref. [17].

Details of the reaction calculations and an assessment of their sensitivity to key parameters are presented in the supplementary text and tables [20]. The intrinsic large- $\ell$  selectivity of the calculated yields, for the optimal parameter set [20] and  $C^2S = 1$ , is shown in Fig. 2 for the  $n(\ell s)J^\pi$  orbitals in the low-energy spectrum of  $^{49}\text{Ca}$ .

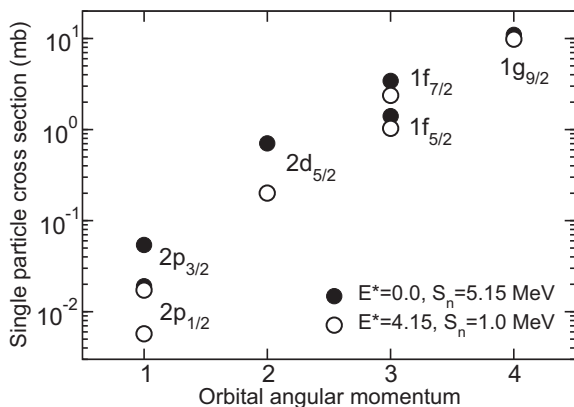


FIG. 2. Neutron-pickup single-particle cross sections (with  $C^2S = 1$ ) for transitions to states in the low-energy spectrum of  $^{49}\text{Ca}$ , showing the large- $\ell$  selectivity of the reaction mechanism. The solid points use the ground-state to ground-state  $Q$  value, with  $S_n$  from  $^{49}\text{Ca}$  of 5.15 MeV [21]. The open points represent transitions to bound excited  $^{49}\text{Ca}$  states near 4 MeV, for which  $S_n = 1$  MeV, showing the effects of the higher  $Q$  value and greater mismatch in this case.

The supplement notes that both the  $n + ^{11}\text{C}$  bound states potential [19,22] and SF (discussed above) are constrained by empirical [charge radius and  $(e, e'p)$ ] data. Following the methods used successfully in intermediate-energy nucleon-removal reactions [23,24], the  $n + ^{48}\text{Ca}$  bound states potential geometry and the entrance and exit channel distorting potentials are constrained by theoretical considerations, through the use of Skyrme Hartree-Fock (HF) calculations [25] with their excellent reproduction of nuclear sizes and densities systematics, to produce an *optimal* parameter set. We show that changes to  $R_{95}$ , the ratio of the calculated  $9/2^+$  (4018 keV) and  $5/2^-$  (3991 keV)  $^{49}\text{Ca}$  final state yields, is (a) very insensitive to significant changes in the densities used to construct the entrance and exit channel distortions, with  $\delta R_{95}$  of less than 1%, and (b) that changes to  $R_{95}$  scale with changes  $\delta r_0$  to the assumed radius parameters of the  $n + ^{48}\text{Ca}$  bound states potentials as  $\delta R_{95}(\%) \approx 1.5 \delta r_0(\%)$ . Since  $\delta r_0(\%)$  of 8%–10% represents very significant corrections to the HF values, this sensitivity drives a modest uncertainty in the deduced  $R_{95}$  of <15%.

The spectroscopic factors  $C^2S$  of the bound ( $^{48}\text{Ca}(0^+) \otimes n(\ell s)J$ ) final-state configurations are discussed in the following. The partial cross sections  $\sigma_{JM}$  to individual  $^{49}\text{Ca}(J^\pi)$  spin projections, with respect to the beam-direction quantization axis, and their fractional populations,  $P_J(M) = \sigma_{JM} / \sum_M \sigma_{JM}$ , are provided by the same reaction calculations. The  $P_J(M)$  of the dominant large- $\ell$  transitions are peaked about  $M \approx 0$ , both exclusively and inclusively with respect to  $I^\pi$ , indicating that these less-mismatched transfers take place predominantly in the reaction plane defined by the asymptotic entrance and exit channel momenta. With the position sensitivity of GRETINA, and the exceptionally clean  $^{49}\text{Ca}$   $\gamma$ -ray spectrum, we can test this aspect of the reaction theory. We explore the  $\gamma$ -ray angular distributions induced by the alignment of excited states through the  $M$ -substate populations  $P_J(M)$ , establishing an approach to probe

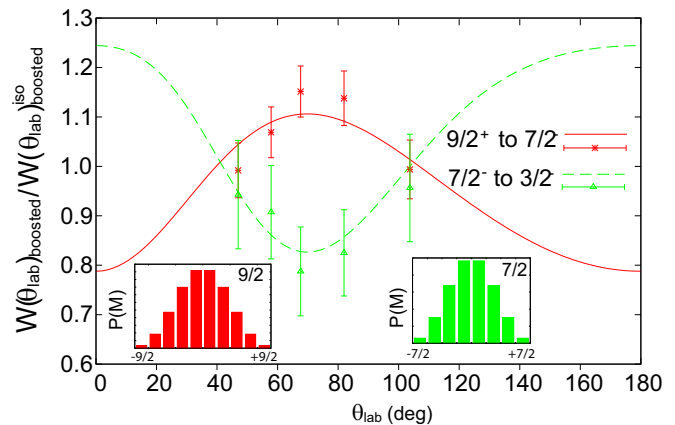


FIG. 3. Measured  $\gamma$ -ray angular distributions for the  $9/2^+ \rightarrow 7/2^- \rightarrow 3/2^-$  ( $E1$ : 660 keV to  $E2$ : 3385 keV) cascade. The  $9/2^+$  state is dominantly fed directly in the reaction and the  $7/2^-$  state is populated essentially exclusively via the 660 keV transition from the  $9/2^+$  state. The calculated angular distributions assuming the specified spins and pure multiplicities are shown. The input  $M$ -substate distribution,  $P_J(M)$ , of the  $9/2^+$  state was taken from the reaction calculations while  $P_J(M)$  for the  $7/2^-$  state was calculated from the angular-momentum coupling and  $P_J(M)$  of the feeding state.

angular momentum and multiplicity assignments in these high-luminosity, inverse-kinematics reactions.

Figure 3 shows the angular distributions of the 660 keV ( $9/2^+ \rightarrow 7/2^-$ ; pure  $E1$  multipolarity) and 3358 keV ( $7/2^- \rightarrow 3/2^-$ ; pure  $E2$  multipolarity) transitions. As we show later, the  $9/2^+$  state is directly populated in the pickup with negligible indirect feeding, while the  $7/2^-$  state is not populated in the pickup and is fed 100% by the  $9/2^+$  state through the 660 keV transition. Using  $P_{9/2}(M)$  from the reaction theory, and with  $P_{7/2}(M)$  deduced from  $P_{9/2}(M)$  and the  $E1$  multipolarity of the connecting transition, the  $\gamma$ -ray angular distributions in the laboratory frame are calculated following Ref. [26]. Those distributions, normalized to a boosted, isotropic angular distribution, are shown as the solid red and green dashed curves in Fig. 3. For the data points in the same figure, full-energy peak intensities of the respective transitions in GRETINA were determined from spectra restricted to five angle ranges, with statistics-optimized widths of 15°–40°. GEANT4 simulations [27] were used to estimate the in-beam efficiency of GRETINA in the angle ranges used and at the respective  $\gamma$ -ray energies, assuming isotropic emission in the rest frame of  $^{49}\text{Ca}$ . The determined intensities per angle bin were then properly normalized by using the simulation results. The agreement between data and calculation is excellent, demonstrating the potential of angular distribution analyses for the purpose of  $J^\pi$  assignments and confirming the amount of alignment introduced by this type of transfer reaction. An accurate determination of the partial cross sections to excited states requires these significant angular-distribution effects to be taken into account. Previous work using the SeGA array in its standard configuration (see Fig. 20 of Ref. [1]) was insensitive to angular-distribution effects. There, only small angle ranges centered on 90° and 37°, near the crossing points of the angular distribution curves in the NSCL velocity regime,

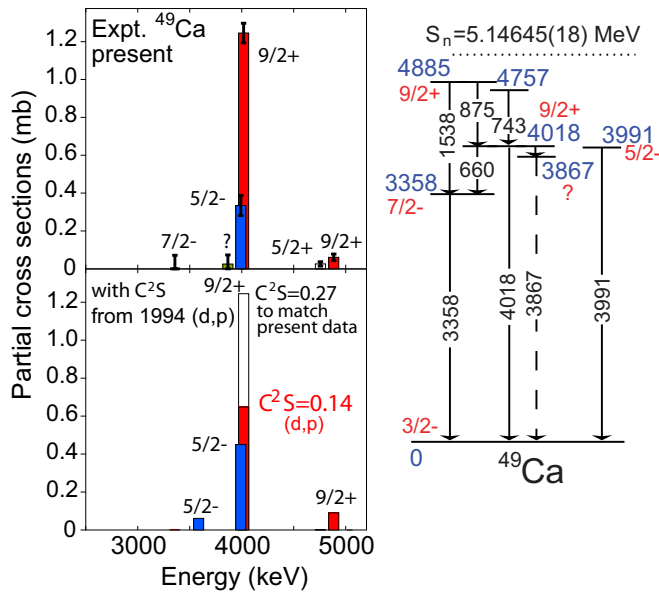


FIG. 4. Measured cross sections compared to calculations that use the reaction theory outlined above and spectroscopic factors from Ref. [6]. While the  $f_{5/2}$  and high-lying  $g_{9/2}$  strengths are consistent, we deduce a higher  $g_{9/2}$  spectroscopic strength of  $C^2S = 0.27(1)_{\text{stat}}$  at 4 MeV.

were covered by the detectors, minimizing uncertainties due to unknown angular distributions.

Exclusive cross sections for the population of individual final excited states were deduced from efficiency-corrected intensities, taking into account the known level scheme in Fig. 4. The Lorentz boost including the angular distributions were folded into the GRETINA efficiencies by using the calculated  $P_J(M)$  and the pure  $E2$ ,  $E1$ , and  $E3$  multipolarities of the 3358, 660, and 4018 keV transitions. A multipole mixing ratio of  $\delta = -1.53$  from the  $fp$  shell model was used for the  $5/2^- \rightarrow 3/2^-$  transition at 3991 keV; the  $\delta$  is high because one expects a rather dominant  $E2$  transition, the competing  $M1$  decay being hindered with  $\Delta\ell = 2$ . An isotropic emission was assumed for all other transitions that are essentially of negligible intensity. With the strong alignment observed in pickup and when using the full angular range of GRETINA, the effect of the angular distributions on the efficiency is observed to be as large as 10%–20% relative to the assumption of isotropic emission.

The  $9/2^+$  state at 4018 keV presents the strongest signal in our spectrum. According to Ref. [13], this state decays with a 660 keV transition [84(1)% branch] to a  $7/2^-$  state, with a 150 keV transition [6.7(8)%] to a state of unknown spin and parity at 3867 keV and to the ground state with a branch that carries only 9.2(8)% of the intensity. We observe all three transitions and our  $I(150)/I(660) = 9(2)\%$  agrees within uncertainty with the literature value (10% systematic uncertainty was added to the statistical uncertainty to account for the unknown angular distribution of the 150 keV transition). The 4018 keV transition forms a doublet with the 3991 keV ground-state decay of the  $5/2^-$  state. The literature branching ratio from Ref. [13] was used to disentangle the intensities, attributing less than 20% of the counts in the peak at 4 MeV

to the  $9/2^+$  to  $3/2^-$   $E3$  transition. This is in contrast to classic modest-resolution, charged-particle-tagged transfer reactions, where the entire spectroscopic strength signal at 4 MeV is obscured by this excitation energy doublet. We note that the 4 MeV  $9/2^+$  state of  $^{49}\text{Ca}$  is of complex nature, suspected to carry [ $^{48}\text{Ca}(3^-) \otimes \nu p_{3/2}$ ] core-coupled configurations [12,13] as well as  $\nu g_{9/2}$  single-particle strength. Our beam energy suppresses two-step processes and the high- $\ell$  selectivity would further suppress this core-coupled component, even if a two-step process were to occur.

The measured cross sections for all states populated in the  $^{12}\text{C}$ -induced one-neutron pickup to  $^{49}\text{Ca}$  are displayed in Fig. 4 and are compared to the reaction calculations discussed above. The calculations use the  $C^2S$  deduced from the most recent charged-particle-tagged ( $d, p$ ) transfer measurement, performed at 56 MeV deuteron beam energy [6]. As can be seen, only two states are populated with significant strength, the  $5/2^-$  state at 3.991 MeV and the  $9/2^+$  state at 4.018 MeV. The measured cross section to the  $5/2^-$  state, corresponding to  $C^2S = 0.62(10)_{\text{stat}}$ , is close to the spectroscopic strength ( $C^2S = 0.84$ ) deduced from the light-ion-induced reaction, while the measured cross section for population of the  $9/2^+$  state requires a  $C^2S(g_{9/2}) = 0.27(1)_{\text{stat}}$  that is twice that deduced in Ref. [6].

Our deduced ratio of spectroscopic strengths,  $S_{95} = C^2S(g_{9/2})/C^2S(f_{5/2}) = 0.435(72)_{\text{stat}}$ , mirrors recent large-scale shell-model calculations [28] carried out in the full  $sd + fp + sdg$  model space, which give  $S_{95}^{SM} = 0.42/0.93 = 0.452$ . In these calculations, (i) natural- and unnatural-parity states are calculated from the full  $0\hbar\omega$  and  $1\hbar\omega$  configurations, (ii) the effective interaction is constructed by analogy to the SDPF-MU interaction: USD ( $sd$ ) + GXPF1B ( $pf$ ) + (refined)  $V_{\text{MU}}$  (for the remaining two-body matrix elements) [28], and (iii) the single-particle energy of the  $g_{9/2}$  orbital was chosen to reproduce the excitation energy of the  $^{51}\text{Ti}(9/2^+)$  state, for which  $C^2S$  was measured to be reasonably large [29]. The calculated  $C^2S$  of 0.47 agrees well with the experimental values of 0.54 or 0.37 for  $^{51}\text{Ti}$  [29]. The single-particle energies (SPEs) of the other  $sdg$  orbitals follow schematic spin-orbit splitting, not affecting  $C^2S(g_{9/2})$ .

We note that the shell-model calculations are sensitive to the  $E3$  effective charges used and, for the present case, these were fit to the  $B(E3; 3_1^- \rightarrow 0_1^+)$  value in  $^{48}\text{Ca}$ . These calculations predict  $C^2S(9/2^+) = 0.42$  for the 4 MeV  $^{49}\text{Ca}$  state and also describe its octupole-coupled nature, with  $B(E3; 9/2_1^+ \rightarrow 3/2_1^-) = 6.3$  Wu, consistent with the measured value of 7.9(2.0) Wu [12]. The energy of the  $^{49}\text{Ca}$   $9/2_1^+$  state is also reasonably described ( $E_x = 3.803$  MeV calculated vs  $E_x = 4.018$  MeV measured). In the future, the  $B(E3)$  strength together with the  $g_{9/2}$  spectroscopic factor allow fine tuning of the  $g_{9/2}$  single-particle energy to which both quantities are sensitive. In this shell-model framework, similarly to the  $3_1^-$  levels in  $^{50,52}\text{Ca}$  [30,31], the  $^{49}\text{Ca}(9/2^+, 4 \text{ MeV})$  state is a strongly mixed configuration of  $sd$ - $pf$  (49%) and  $pf$ - $sdg$  excitations (51%). This is due to the Fermi surface moving to the  $p_{3/2}$  orbital and above, reducing the effective shell gap to the  $g_{9/2}$  orbital as neutrons are added to  $^{48}\text{Ca}$ .

In summary, we studied a highly selective intermediate-energy inverse-kinematics heavy-ion-induced neutron-pickup reaction, in combination with  $\gamma$ -ray spectroscopy. We demonstrate that the pickup from the  $^{12}\text{C}$  target leads to significant alignment, allowing the use of  $\gamma$ -ray angular distributions for the determination of spin values in the regime of high-luminosity fast-beam experiments. In the crucial Ca isotopic chain, the ratio  $S_{95}$  of spectroscopic strengths was extracted, including an assessment of the sensitivities and uncertainties of the reaction theory. The ratio agrees with full  $sd + pf + sdg$  valence-space shell-model calculations, where the complex structure and octupole degree of freedom of the  $^{49}\text{Ca}(9/2^+, 4 \text{ MeV})$  state is well described. The result will provide an important benchmark for calculations based on *ab initio* approaches, once these are able to describe the interplay of

octupole and single-particle degrees of freedom in the Ca isotopic chain.

### ACKNOWLEDGMENTS

GRETINA was funded by the DOE, Office of Science. Operation of the array at NSCL was supported by NSF under Cooperative Agreement PHY-1102511 (NSCL) and DOE under Grant No. DE-AC02-05CH11231 (LBNL). We further acknowledge support from NSF Grant No. PHY-1404442 (NSCL). D.H. acknowledges funding from NSF Grant No. PHY-1203100. J.A.T. acknowledges support of the Science and Technology Facilities Council (UK) Grants No. ST/J000051 and No. ST/L005743. Y.U. acknowledges support from JSPS KAKENHI (Japan), Grant No. 15K05094.

- 
- [1] A. Gade and T. Glasmacher, *Prog. Part. Nucl. Phys.* **60**, 161 (2008).
- [2] A. Gade, J. A. Tostevin, T. Baugher, D. Bazin, B. A. Brown, C. M. Campbell, T. Glasmacher, G. F. Grinyer, S. McDaniel, K. Meierbachtol, A. Ratkiewicz, S. R. Stroberg, K. A. Walsh, D. Weisshaar, and R. Winkler, *Phys. Rev. C* **83**, 054324 (2011).
- [3] D. Brink, *Phys. Lett. B* **40**, 37 (1972).
- [4] W. R. Phillips, *Rep. Prog. Phys.* **40**, 345 (1977).
- [5] S. Takeuchi, T. Motobayashi, Y. Togano, M. Matsushita, N. Aoi, K. Demichi, H. Hasegawa, and H. Murakami, *Nucl. Instrum. Methods Phys. Res., Sect. A* **763**, 596 (2014).
- [6] Y. Uozumi, O. Iwamoto, S. Widodo, A. Nohtomi, T. Sakae, M. Matoba, M. Nakano, T. Maki, and N. Koori, *Nucl. Phys. A* **576**, 123 (1994).
- [7] D. J. Morrissey *et al.*, *Nucl. Instrum. Methods Phys. Res., Sect. B* **204**, 90 (2003).
- [8] D. Bazin *et al.*, *Nucl. Instrum. Methods Phys. Res., Sect. B* **204**, 629 (2003).
- [9] S. Paschalis *et al.*, *Nucl. Instrum. Methods Phys. Res., Sect. A* **709**, 44 (2013).
- [10] S. R. Stroberg, A. Gade, J. A. Tostevin, V. M. Bader, T. Baugher, D. Bazin, J. S. Berryman, B. A. Brown, C. M. Campbell, K. W. Kemper, C. Langer, E. Lunderberg, A. Lemasson, S. Noji, F. Recchia, C. Walz, D. Weisshaar, and S. J. Williams, *Phys. Rev. C* **90**, 034301 (2014).
- [11] S. Raman, C. W. Nestor, and P. Tikkanen, *At. Data Nucl. Data Tables* **78**, 1 (2001).
- [12] D. Montanari, S. Leoni, D. Mengoni, G. Benzoni, N. Blasi *et al.*, *Phys. Lett. B* **697**, 288 (2011).
- [13] D. Montanari, S. Leoni, D. Mengoni, J. J. Valiente-Dobon, G. Benzoni *et al.*, *Phys. Rev. C* **85**, 044301 (2012).
- [14] M. C. Mermaz, E. Tomasi-Gustafsson, B. Berthier, R. Lucas, J. Gastebois, A. Gillibert, A. Miczaika, A. Boucenna, L. Kraus, I. Linck, B. Lott, R. Rebmeister, N. Schulz, J. C. Sens, and C. Grunberg, *Phys. Rev. C* **37**, 1942 (1988).
- [15] J. S. Winfield, E. Adamides, Sam M. Austin, G. M. Crawley, M. F. Mohar, C. A. Ogilvie, B. Sherrill, M. Torres, G. Yoo, and A. Nadasen, *Phys. Rev. C* **39**, 1395 (1989).
- [16] I. J. Thompson, Computer code FRESKO, available at <http://www.fresco.org.uk/index.htm>; *Comput. Phys. Rep.* **7**, 167 (1988).
- [17] G. van der Steenhoven, H. P. Blok, E. Jans, M. de Jong, L. Lapikas, E. N. M. Quint, and P. K. A. de Witt Huberts, *Nucl. Phys. A* **480**, 547 (1988).
- [18] E. K. Warburton and B. A. Brown, *Phys. Rev. C* **46**, 923 (1992).
- [19] B. A. Brown, P. G. Hansen, B. M. Sherrill, and J. A. Tostevin, *Phys. Rev. C* **65**, 061601 (2002).
- [20] See Supplemental Material at <http://link.aps.org/supplemental/10.1103/PhysRevC.93.031601> for further details of the reaction model parameters and the cross-section sensitivities.
- [21] M. Wang, G. Audi, A. H. Wapstra, F. G. Kondev, M. MacCormick, X. Xu, and B. Pfeiffer, *Chin. Phys. C* **36**, 1603 (2012).
- [22] R. H. Bassel *et al.*, *J. Phys. G: Nucl. Phys.* **8**, 1215 (1982).
- [23] A. Gade, P. Adrich, D. Bazin, M. D. Bowen, B. A. Brown, C. M. Campbell, J. M. Cook, T. Glasmacher, P. G. Hansen, K. Hosier, S. McDaniel, D. McGlinchery, A. Obertelli, K. Siwek, L. A. Riley, J. A. Tostevin, and D. Weisshaar, *Phys. Rev. C* **77**, 044306 (2008).
- [24] J. A. Tostevin, G. Podolyak, B. A. Brown, and P. G. Hansen, *Phys. Rev. C* **70**, 064602 (2004); J. A. Tostevin and B. A. Brown, *ibid.* **74**, 064604 (2006).
- [25] B. A. Brown, *Phys. Rev. C* **58**, 220 (1998).
- [26] H. Olliver, T. Glasmacher, and A. E. Stuchbery, *Phys. Rev. C* **68**, 044312 (2003).
- [27] L. A. Riley, UCGretina GEANT4, Ursinus College (unpublished).
- [28] Y. Utsuno, T. Otsuka, B. A. Brown, M. Honma, T. Mizusaki, and N. Shimizu, *Prog. Theor. Phys. Suppl.* **196**, 304 (2012).
- [29] P. Wilhelm, Ole Hansen, J. R. Comfort, C. K. Bockelman, P. D. Barnes, and A. Sperduto, *Phys. Rev.* **166**, 1121 (1968).
- [30] R. A. Broglia, P. Federman, Ole Hansen, K. Hehl, and C. Riedel, *Nucl. Phys. A* **106**, 421 (1968).
- [31] A. Gade, R. V. F. Janssens, D. Bazin, R. Broda, B. A. Brown, C. M. Campbell, M. P. Carpenter, J. M. Cook, A. N. Deacon, D.-C. Dinca, B. Fornal, S. J. Freeman, T. Glasmacher, P. G. Hansen, B. P. Kay, P. F. Mantica, W. F. Mueller, J. R. Terry, J. A. Tostevin, and S. Zhu, *Phys. Rev. C* **74**, 021302(R) (2006).